

The effect of an external magnetic field on oscillatory instability of convective flows in a rectangular cavity

A. Yu. Gelfgat and P. Z. Bar-Yoseph

Computational Mechanics Laboratory, Faculty of Mechanical Engineering, Technion—Israel Institute of Technology, Haifa, 32000, Israel

(Received 1 March 2000; accepted 26 April 2001)

The present study is devoted to the problem of onset of oscillatory instability in convective flow of an electrically conducting fluid under an externally imposed time-independent uniform magnetic field. Convection of a low-Prandtl-number fluid in a laterally heated two-dimensional horizontal cavity is considered. Fixed values of the aspect ratio (length/height=4) and Prandtl number ($Pr=0.015$), which are associated with the horizontal Bridgman crystal growth process and are commonly used for benchmarking purposes, are considered. The effect of a uniform magnetic field with different magnitudes and orientations on the stability of the two distinct branches (with a single-cell or a two-cell pattern) of the steady state flows is investigated. Stability diagrams showing the dependence of the critical Grashof number on the Hartmann number are presented. It is shown that a vertical magnetic field provides the strongest stabilization effect, and also that multiplicity of steady states is suppressed by the electromagnetic effect, so that at a certain field level only the single-cell flows remain stable. An analysis of the most dangerous flow perturbations shows that starting with a certain value of the Hartmann number, single-cell flows are destabilized inside thin Hartmann boundary layers. This can lead to destabilization of the flow with an increase of the field magnitude, as is seen from the stability diagrams obtained. Contrary to the expected monotonicity of the stabilization process with an increase of the field strength, the marginal stability curves show nonmonotonic behavior and may contain hysteresis loops. © 2001 American Institute of Physics. [DOI: 10.1063/1.1383789]

I. INTRODUCTION

The externally imposed magnetic field is a widely used tool for control of melt flow in bulk crystal growth of semiconductors. One of the main purposes of the electromagnetic control is stabilization of the flow and suppression of the oscillatory instabilities arising at certain values of the control parameters. Such suppression was used in the pioneer experiments of Hurle,^{1,2} and since then has been widely used in the processing of bulk semiconductor monocrystals³ and other technological processes involving metal melting and solidification. There exist numerous studies devoted to numerical modeling of the electromagnetic stabilization of convective flows in several different configurations and at some fixed values of the governing parameters (see Refs. 3–13 and references therein). However, to the best of our knowledge, there are no numerical studies reporting a validated dependence of the critical Grashof number on the magnitude and orientation of the magnetic field over a relatively wide range of parameters. Such a dependence is obtained in the present study for a particular geometry of the flow region and for $Pr=0.015$, where Pr is the Prandtl number. The model considered (convection in a horizontally elongated rectangular cavity) is usually associated with the horizontal Bridgman crystal growth process. An investigation of the electromagnetic stabilization of convection in a rather simple numerical model leads to several important qualitative conclusions, which will be valid also for more complicated configurations

and therefore are relevant to the technological processes mentioned above. Thus, the electromagnetic force changes the flow pattern so that the convective circulation and the largest values of the temperature gradient are located in thin Hartmann layers which are boundary layers adjacent to the walls normal to the magnetic field. Consequently, the instability sets in inside the boundary layers where the convective flow is most intensive. It is shown that contrary to the expected monotonic increase of the critical Grashof number with the magnetic field strength, the corresponding marginal stability curves show nonmonotonic behavior and may contain hysteresis loops. In particular, we show that in spite of the strong damping of the flow a stronger magnetic field does not always provide better stabilization of a steady flow. It was quite unexpectedly found that the critical Grashof number can be almost halved as the field strength increases. This leads to the problem of determining the optimal stabilizing field magnitude, which has not hitherto been considered or formulated. Furthermore, we show that the electromagnetic effect suppresses the multiplicity of possible steady state flows¹⁴ so that only single-cell flows remain stable under a sufficiently strong electromagnetic force.

Following the configuration of an experimental setup,¹ a widely used computational model represents convection of a low-Prandtl-number fluid in a laterally heated rectangular cavity. The whole system is subjected to an externally imposed constant and uniform magnetic field whose orientation and magnitude can be varied. The considered problem is

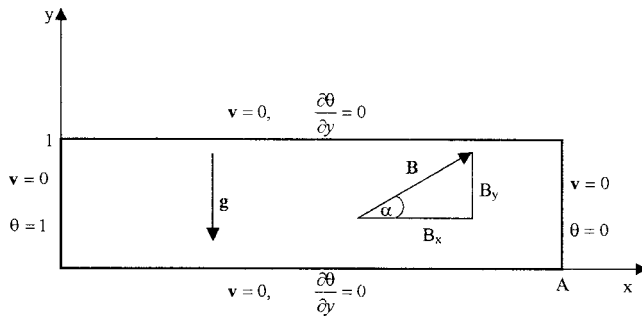


FIG. 1. Sketch of the problem.

shown schematically in Fig. 1. Several experimental^{4–6} and numerical^{4,7–11} studies considered the influence of the magnetic field on the damping of steady convection and heat transfer in a rectangular cavity. However, in spite of the numerous studies devoted to the oscillatory instability of low-Prandtl-number fluid convection in rectangular cavities,^{14–18} there is a marked shortage of numerical studies regarding the electromagnetic effect on the onset of instability. Most of the numerical studies^{4,7–11} deal with changes in steady state flow patterns. To the best of our knowledge, Gelfgat¹⁹ made the only attempt to obtain a relationship between the critical Grashof number and the strength of the magnetic field by low-mode modeling. However, as is shown here, numerical models with poor spatial resolution, such as those with a small number of spectral modes or coarse grids, are incapable of resolving the Hartmann layers and therefore fail to yield the correct perturbation pattern.

In the present paper the effect of an externally imposed magnetic field on the stability of a steady convective flow is studied by linear stability analysis. The completed study yielded stability diagrams showing the dependence of the critical Grashof number (corresponding to the steady–oscillatory transition) and critical circular frequency of oscillations (frequency of the oscillatory flow at the critical value of Grashof number) on the Hartmann number for the considered problem. To simplify all additional effects and following our previous studies,^{14–17} a simple model of convection in a laterally heated cavity is considered. We use an aspect (length-to-height) ratio of 4 and $Pr=0.015$, which correspond to the widely used benchmark problem.¹⁸ A convergence study involving different values of the Hartmann number and different orientations of the magnetic field shows that accurate modeling of the electromagnetic effect requires better numerical resolution than the one that suffices for different cases of pure buoyancy convection.^{14–17} This contradicts the common expectation that electromagnetic damping of the convective flow makes numerical modeling easier. The results obtained lead to the already mentioned conclusions about the behavior of the multiple solutions, marginal stability curves, and the most dangerous perturbations patterns.

II. GOVERNING EQUATIONS

Convective flow of a Boussinesq fluid with kinematic viscosity ν , density ρ , thermal diffusivity χ , and electrical conductivity σ in a two-dimensional cavity of length L and

height H is considered. The problem is shown schematically in Fig. 1. The vertical boundaries of the cavity have uniform temperatures θ_{hot} and θ_{cold} , respectively, while the horizontal boundaries are thermally insulated. The cavity is subjected to a uniform magnetic field $\mathbf{B}=B_x\mathbf{e}_x+B_y\mathbf{e}_y$ (where B_x and B_y are space independent) of constant magnitude $B_0=\sqrt{B_x^2+B_y^2}$, and \mathbf{e}_x and \mathbf{e}_y are unit vectors for a Cartesian coordinate system. The orientation of the magnetic field forms an angle α with the horizontal axis [$\tan(\alpha)=B_y/B_x$]. The electric current \mathbf{J} and the electromagnetic force \mathbf{F}_{EM} are defined by

$$\mathbf{J}=\sigma(-\nabla\varphi+\mathbf{v}\times\mathbf{B}), \quad (1a)$$

$$\nabla\cdot\mathbf{J}=0, \quad (1b)$$

$$\mathbf{F}_{\text{EM}}=\mathbf{J}\times\mathbf{B}, \quad (1c)$$

where φ is the electric potential and $\mathbf{v}=v_x\mathbf{e}_x+v_y\mathbf{e}_y$ is the fluid velocity. Here Eq. (1a) is Ohm's law and Eq. (1b) is the conservation of electric current. With electrically insulated boundaries in the present two-dimensional flow, the electric potential φ is constant and

$$\mathbf{J}=\sigma[\mathbf{v}\times\mathbf{B}], \quad (2a)$$

$$\mathbf{F}_{\text{EM}}=\sigma[\mathbf{v}\times\mathbf{B}]\times\mathbf{B}. \quad (2b)$$

The flow is described by the momentum, continuity and energy equations in a Cartesian coordinate system. Using the scales H , H^2/ν , ν/H , $\rho(\nu/H)^2$, and B_0 for length, time, velocity, pressure and magnetic field, respectively, and $\theta=(\theta-\theta_{\text{cold}})/(\theta_{\text{hot}}-\theta_{\text{cold}})$ for nondimensionalization of the temperature, the dimensionless equations governing the velocity \mathbf{v} , temperature θ and pressure p in the rectangular domain $0\leq x\leq A$, $0\leq y\leq 1$ are

$$\begin{aligned} \frac{\partial v_x}{\partial t}+v_x\frac{\partial v_x}{\partial x}+v_y\frac{\partial v_x}{\partial y} \\ =-\frac{\partial p}{\partial x}+\frac{\partial^2 v_x}{\partial x^2}+\frac{\partial^2 v_x}{\partial y^2} \\ +\text{Ha}^2[v_y\cos(\alpha)\sin(\alpha)-v_x\sin^2(\alpha)], \end{aligned} \quad (3)$$

$$\begin{aligned} \frac{\partial v_y}{\partial t}+v_x\frac{\partial v_y}{\partial x}+v_y\frac{\partial v_y}{\partial y} \\ =-\frac{\partial p}{\partial y}+\frac{\partial^2 v_y}{\partial x^2}+\frac{\partial^2 v_y}{\partial y^2} \\ +\text{Gr}\theta+\text{Ha}^2[v_x\cos(\alpha)\sin(\alpha)-v_y\cos^2(\alpha)], \end{aligned} \quad (4)$$

$$\frac{\partial v_x}{\partial x}+\frac{\partial v_y}{\partial y}=0, \quad (5)$$

$$\frac{\partial \theta}{\partial t}+v_x\frac{\partial \theta}{\partial x}+v_y\frac{\partial \theta}{\partial y}=\frac{1}{\text{Pr}}\left(\frac{\partial^2 \theta}{\partial x^2}+\frac{\partial^2 \theta}{\partial y^2}\right). \quad (6)$$

Here $A=L/H$ is the aspect ratio of the cavity, $\text{Gr}=\beta g(\theta_{\text{hot}}-\theta_{\text{cold}})H^3/\nu^2$ the Grashof number, $\text{Pr}=\nu/\chi$ the Prandtl number, $\text{Ha}=B_0H\sqrt{\sigma/\rho\nu}$ the Hartmann number, g gravitational acceleration, and β the thermal expansion coefficient.

No-slip boundary conditions are imposed at all boundaries,

$$\mathbf{v}=0, \text{ at } x=0, A \text{ and } y=0, 1; \tag{7}$$

constant temperatures are imposed at the vertical boundaries,

$$\theta=1, \text{ at } x=0, \tag{8a}$$

$$\theta=0, \text{ at } x=A, \tag{8b}$$

and zero heat fluxes are imposed at the horizontal boundaries,

$$\partial\theta/\partial y=0, \text{ at } y=0, 1. \tag{9}$$

The effect of the induced electric currents on the imposed field and the Joulean heating are neglected. This is justified by an estimation of the nondimensional parameters characteristic for liquid metals and semiconductors. In fact, the ratio of the induced and imposed magnetic fields is defined by the magnetic Prandtl number $Pr_m = \mu\sigma\nu$, where μ is the magnetic permeability. For liquid metals and semiconductors²⁰ $Pr_m \sim 10^{-7}$. The Joulean heating is described by the dimensionless source term

$$q = \frac{H^2}{c_p\rho\nu(\theta_{\text{hot}}-\theta_{\text{cold}})} \frac{\mathbf{J}^2}{\sigma} = \frac{\sigma\nu B_0^2}{c_p\rho(\theta_{\text{hot}}-\theta_{\text{cold}})} [\mathbf{v}\times\mathbf{B}]^2 = D \frac{Ha^2}{Gr} [\mathbf{v}\times\mathbf{B}]^2, \tag{10}$$

$$D = \frac{g\beta H}{c_p}.$$

For liquid metals and semiconductors the heat capacity c_p is of order 10^2 J/kg K, and the thermal expansion coefficient β of order 10^{-3} K⁻¹, so that for H of order 1 m the dimensionless parameter D is of order 10^{-4} . Furthermore, we consider cases with $Ha < 10^2$ and $Gr > 10^5$. Therefore, the coefficient $D Ha^2/Gr$ is of order 10^{-5} or smaller, and the term in question can be neglected.

III. NUMERICAL METHOD AND TEST CALCULATIONS

Following our previous studies,¹⁴⁻¹⁷ we use the global Galerkin method for the calculation of steady flows, analysis of their stability and weakly nonlinear analysis of slightly supercritical flows. The velocity and temperature are approximated by the truncated series

$$\mathbf{v} = \sum_{i=1}^{N_x} \sum_{j=1}^{N_y} c_{ij}(t) \mathbf{u}_{ij}(x,y), \tag{11a}$$

$$\theta = (1-x) + \sum_{i=1}^{N_x} \sum_{j=1}^{N_y} d_{ij}(t) q_{ij}(x,y), \tag{11b}$$

where $c_{ij}(t)$ and $d_{ij}(t)$ are time-dependent coefficients to be found, and N_x and N_y the number of basis functions used for approximation in the x - and y -directions, respectively. Here $\mathbf{u}_{ij}(x,y)$ and $q_{ij}(x,y)$ are vector and scalar basis functions, respectively, defined as linear superpositions of Chebyshev polynomials satisfying *a priori* the boundary conditions and the continuity equation. The subscripts i and j represent the order of the first polynomial in the linear superpositions in

the x - and y -directions, respectively. All terms of Eqs. (3), (4) and (6) are evaluated as Galerkin projections on the bases (11). The corresponding inner products are evaluated analytically. The pressure is eliminated by projection of the pressure gradient on the divergence-free velocity basis.^{14,17} The stream function ψ , defined by $v_x = -\partial\psi/\partial y$, $v_y = \partial\psi/\partial x$, is calculated as the integral of the velocity series (11) and used for evaluation of the streamlines.

According to the linear stability approach, the calculated steady state flow is subjected to all possible infinitesimally small perturbations, characterized by a complex time growth rate λ (each unknown function being supposed to behave in time as $\sim e^{\lambda t}$) and a spatially distributed amplitude. This results in an eigenvalue problem where λ is considered as the eigenvalue and the perturbation amplitude as the eigenvector. The instability onset is associated with values of the governing parameters (called *critical values*) for which the real part of λ exceeds zero, and the imaginary part characterizes the time behavior of the instability. Namely, if $\text{Re}(\lambda)=0$ and $\omega_{cr} = \text{Im}(\lambda)$, then $\omega_{cr}=0$ corresponds to a transition from one steady state to another, while $\omega_{cr}\neq 0$ indicates a transition from a steady to an oscillatory state. In the latter case the value of ω_{cr} represents the circular frequency of oscillation and is called the *critical frequency*. The eigenvector corresponding to the eigenvalue $\lambda = i\omega_{cr}$ is called the *most dangerous perturbation*. In case of a supercritical Hopf bifurcation, a slightly supercritical oscillatory state can be approximated as

$$\{\mathbf{v}(x,y,t), \theta(x,y,t)\} \approx \{\mathbf{v}_0(x,y), \theta_0(x,y)\} + \epsilon\{\tilde{\mathbf{v}}(x,y), \tilde{\theta}(x,y)\} \exp(i\omega_{cr}t), \tag{12}$$

where $\{\mathbf{v}_0, \theta_0\}$ is the steady flow at $Gr=Gr_{cr}$, $\{\tilde{\mathbf{v}}(x,y), \tilde{\theta}(x,y)\}$ the most dangerous perturbation, Gr_{cr} the critical Grashof number; ϵ the amplitude of the perturbation calculated as a function of the supercriticality $(Gr-Gr_{cr})/Gr_{cr}$ via the weakly nonlinear analysis.¹⁷ Note that the perturbation is a complex function and its absolute value, to within multiplication by a constant, coincides with the amplitude of flow oscillations corresponding to a slightly supercritical oscillatory state, as follows from Eq. (12).^{14,17}

The complete numerical process consists of (i) calculation of the steady state solution of Eqs. (3)–(9), (ii) calculation of the critical Grashof number Gr_{cr} depending on all other governing parameters, and (iii) calculation of the dependence of the amplitude of the most dangerous perturbation on the supercriticality.¹⁷ To validate the results we solve the full unsteady problem, using another solver formulated in primitive variables and based on second-order finite volume discretization in space and second-order three-time-level discretization in time. Time-stepping is done using the SIMPLE algorithm. A solution obtained by the Galerkin method was taken as an initial state.

A previous study¹⁴ on the stability of convective flows without an electromagnetic effect for $A=4$ and $Pr=0.015$ showed that there are two distinct steady-state flow patterns. In that study Gelfgat *et al.* showed that among a steady flow with a single convective circulation, another steady-state

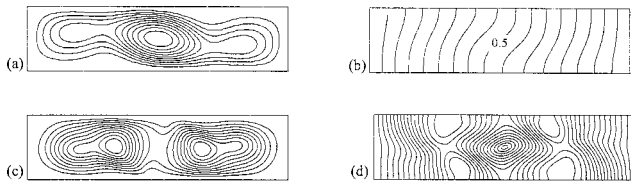


FIG. 2. Single-cell flow without a magnetic field at the critical Grashof number $Gr_{cr}=1.32 \times 10^5$ [point F_2 in Fig. 6(a)]. All contours are equally spaced. (a) Streamlines, $\psi_{min}=0$, $\psi_{max}=79.625$; (b) isotherms, $0 \leq \theta \leq 1$; (c) amplitude of the most dangerous perturbation of the stream function; (d) amplitude of the most dangerous perturbation of the temperature.

branch with two main circulations appears when the Grashof number exceeds $Gr \approx 1.20 \times 10^5$ and remains stable up to $Gr \approx 1.48 \times 10^6$. This phenomenon is demonstrated in Figs. 2(a) and 3(a) which show a single convective circulation for $Gr_{cr}=1.32 \times 10^5$ and two circulations for $Gr_{cr}=1.48 \times 10^6$, respectively, the critical values for two solutions. The isotherms for the circulations in the above figures are presented in Figs. 2(b) and 3(b), respectively. The amplitudes of the most dangerous perturbation of the stream function and the temperature are presented in Figs. 2(c), 2(d), 3(c), and 3(d), respectively. As was mentioned above, the perturbations are defined to within multiplication by a constant; thus the magnitudes of the maximal absolute values have no meaning. The amplitude of the oscillating perturbations can be derived from the weakly nonlinear analysis of the Hopf bifurcation,¹⁷ which is used here for an asymptotic approximation of slightly supercritical oscillatory flows.

For the considered problem of convection in rectangular cavities, convergence of the global Galerkin method was studied in detail.¹⁴⁻¹⁷ Here we focus mainly on the influence of the magnetic field on the convergence of computed critical parameters, and on the steady states calculated at the critical points for $A=4$ and $Pr=0.015$. To compare the convergence with and without a magnetic field, we report the results for $Ha=0$, for $Ha=20$ with $\alpha=0^\circ$, and for $Ha=10$ with $\alpha=90^\circ$, in Tables I, II and III, respectively, which correspond to the steady-state flows and perturbations shown in Figs. 2, 4 and 5, respectively. The tables show the critical Grashof number Gr_{cr} and the corresponding critical oscillation frequency ω_{cr} calculated for different numbers of basis functions in the Galerkin series (11). To characterize the steady-state flows as well, we report the maximal value of the stream function ψ_{max} and the Nusselt number,

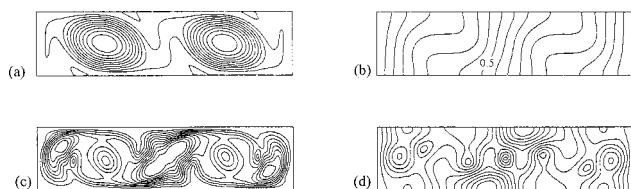


FIG. 3. Two-cell flow without a magnetic field at the critical Grashof number $Gr_{cr}=1.48 \times 10^6$ [point F_3 in Fig. 9(a)]. All contours are equally spaced. (a) Streamlines, $\psi_{min}=-0.5499$, $\psi_{max}=233.45$; (b) isotherms, $0 \leq \theta \leq 1$; (c) amplitude of the most dangerous perturbation of the stream function; (d) amplitude of the most dangerous perturbation of the temperature.

TABLE I. Convergence of the Nusselt number (at $Gr=1.32 \times 10^5$) and critical parameters for $Ha=0$.

N_x	N_y	ψ_{max}	Nu	$Gr_{cr} \times 10^{-5}$	ω_{cr}
40	10	79.73818	1.136835	1.31176	122.420
40	20	79.66010	1.136620	1.32078	123.510
50	20	79.66111	1.136619	1.31981	123.456
60	20	79.66118	1.136619	1.31972	123.446
60	30	79.66116	1.136619	1.31983	123.454
70	30	79.66112			
70	40	79.66112	No	further	change
80	30	79.66113			

$$Nu = \int_0^1 \frac{\partial \theta}{\partial x} \Big|_{x=0} dy, \tag{13}$$

calculated at the hot wall for the critical value of the Grashof number, Gr_{cr} .

As Table I shows, convergence for $Ha=0$ is fast, such that four correct digits of Gr_{cr} and ω_{cr} are already obtainable with 50 and 20 basis functions in the x - and y -directions, respectively. At $N_x=60$ and $N_y=30$ six correct digits are obtainable. Convergence of the steady state is even faster, such that seven correct digits of the Nusselt number and six correct digits of ψ_{max} are obtainable already with 50×20 basis functions.

The imposed magnetic field damps the flow, which leads to an increase of the critical Grashof number. A horizontal field with $Ha=20$ increases the value of Gr_{cr} by approximately a factor of 4, as shown in Table II. Damping of the steady-state flow is still weak, as is seen from the values of ψ_{max} and Nu, which are significantly higher (following the increase of Gr_{cr}) compared with the $Ha=0$ case. This means that the electromagnetic force suppresses perturbations of the flow before significant electromagnetic damping of the steady state has taken place. Therefore, numerical modeling of stability requires an accurate calculation of the steady state together with the corresponding most dangerous perturbation. Table II shows that 60×30 basis functions yield only four correct digits of both the critical parameters and the stream function, and five correct digits of the Nusselt number.

This slowdown of convergence of the critical parameters is even more pronounced for a vertical magnetic field, as is shown in Table III. Here, even a smaller value of the Hartmann number, $Ha=10$, increases Gr_{cr} by two orders of mag-

TABLE II. Convergence of the Nusselt number (at $Gr=5.4 \times 10^6$) and critical parameters for $Ha=20$, $\alpha=0^\circ$.

N_x	N_y	ψ_{max}	Nu	$Gr_{cr} \times 10^{-6}$	ω_{cr}
40	10	362.667	3.4110	5.918	2037
40	20	365.963	3.4374	5.372	1926
50	20	365.975	3.4375	5.367	1925
60	20	365.978	3.4377	5.366	1924
60	30	365.939	3.4377	5.373	1925
70	30	365.946			
70	40	365.946	No	further	change
80	30	365.948			

TABLE III. Convergence of the Nusselt number (at $Gr = 1.6 \times 10^7$) and critical parameters for $Ha=10$, $\alpha=90^\circ$.

N_x	N_y	ψ_{\max}	Nu	$Gr_{cr} \times 10^{-7}$	ω_{cr}
40	10	542.315	8.2628	0.9769	4994
40	20	548.328	8.4661	1.446	5995
50	20	547.874	8.4712	1.473	6054
60	20	547.792	8.4708	1.477	6063
60	30	547.636	8.4692	1.594	6313
60	40	547.610	8.4688	1.593	6310
70	30	547.620	No	1.594	6313
70	40	547.619	further	1.593	6310
80	30	547.619	change	1.594	6313

nitude, but 60×30 basis functions yield only three correct digits of the critical parameters. Convergence of the Nusselt number and the stream function also slows down, while their values corresponding to the critical state, increase rapidly.

Since a 60×30 basis suffices for three or more correct digits in the critical parameters, we can accurately calculate the dependences $Gr_{cr}(Ha)$ and $\omega_{cr}(Ha)$ for a horizontal magnetic field with $Ha \leq 20$ and a vertical magnetic field with $Ha \leq 10$. In view of the slowed convergence, the stability analysis cannot be extended to larger Hartmann numbers. However, recent experimental observations of convective flow in a cylindrical cell²¹ showed that convective oscillations are already damped at the relatively low value of $Ha = 10$.

The reason for the convergence slowdown follows from the flow patterns of flow and the most dangerous perturbation. The critical steady state of the flow, under the horizontal magnetic field, and the corresponding most dangerous perturbation are shown in Fig. 4. The horizontal field generates a vertical electromagnetic force which counteracts any vertical velocity. The strongest damping takes place near the vertical boundaries where the vertical velocity is highest (according to Ref. 18, the maximal absolute values of the vertical velocity in the cross-section $y = 0.5$ are located at $x \approx 0.15$ and $x \approx 3.85$). As a result, the main convective circulation deforms so that the most intensive flow is shifted towards the center and the horizontal boundaries, as shown in Fig. 4(a). Figure 4(b) indicates that heat convection is strong in the central region, while near the vertical boundaries the isotherms remain almost vertical. The perturbations of the stream function and the temperature, located in the core of the flow at $Ha=0$ [Figs. 2(c) and 2(d)], appear to be most

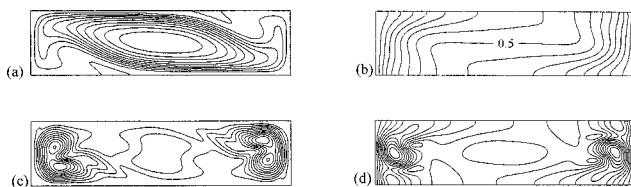


FIG. 4. Single-cell flow under the horizontal magnetic field at the critical Grashof number. $Ha=20$, $\alpha=0^\circ$, $Gr_{cr} = 5.37 \times 10^6$ [point F_4 in Fig. 6(a)]. All contours are equally spaced. (a) Streamlines, $\psi_{\min} = -1.919$, $\psi_{\max} = 365.18$; (b) isotherms, $0 \leq \theta \leq 1$; (c) amplitude of the most dangerous perturbation of the stream function; (d) amplitude of the most dangerous perturbation of the temperature.

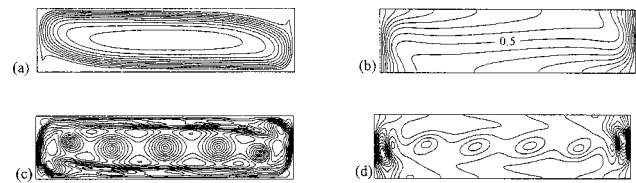


FIG. 5. Single-cell flow under the vertical magnetic field at the critical Grashof number. $Ha=10$, $\alpha=90^\circ$, $Gr_{cr} = 1.59 \times 10^7$. All contours are equally spaced. (a) Streamlines, $\psi_{\min} = -0.563$, $\psi_{\max} = 546.91$; (b) isotherms, $0 \leq \theta \leq 1$; (c) amplitude of the most dangerous perturbation of the stream function; (d) amplitude of the most dangerous perturbation of the temperature.

intensive near the vertical boundaries, where the electromagnetic damping is strongest and the convective circulation is weakened. The slowed convergence of the critical parameters is reflected in the need for correct resolution of the perturbation pattern (containing sharp maxima near the vertical boundaries), while at the same time resolving accurately the steady-state flow at larger values of the Grashof number.

The effect of a vertical magnetic field is quite different as is shown in Fig. 5. The vertical field generates a horizontal electromagnetic force $\mathbf{F}_{EM} = -Ha^2 \nu_x \mathbf{e}_x$, which counteracts the horizontal velocity. Since the cavity is elongated horizontally, for a single convective circulation the maximum horizontal velocity exceeds its vertical counterpart. Therefore, for a given Ha , the electromagnetic damping and stabilization will be stronger for a vertical magnetic field. Thus, for a horizontal field with $Ha=10$ the critical Grashof number is smaller than the one with $Ha=20$ (Table II), and accordingly significantly smaller than its counterpart for a vertical field with $Ha=10$ (Table III). In the case illustrated in Fig. 5, the horizontal velocity, counteracted by the opposing force, forms Hartmann boundary layers near the horizontal boundaries and, via the continuity, near the vertical boundaries as well (the depth of the Hartmann boundary layers decreases proportionally to Ha^{-1} as Ha increases). Ben Hadid *et al.*⁸ showed that depth of the layers adjoining the boundaries parallel to the magnetic field (the vertical ones in the case considered) behaves as $Ha^{-1/2}$. The pattern of the convective circulation shown in Fig. 5(a) is characterized by steep gradients of the stream function near the boundaries. The pattern in Fig. 5(c) also shows a rapid increase of the stream function perturbation inside the boundary layers and several local maxima in the core flow. At the same time the temperature perturbation has two sharp maxima near the vertical boundaries [Fig. 5(d)]. As in the previous case, the steep slowdown of the convergence is reflected in the need to resolve the boundary layers with regard to the velocity and its perturbation, as well as the sharp maxima of the temperature perturbation.

To sum up, it can be concluded that numerical modeling of the magnetic field effect necessitated resolution of the Hartmann layers, which in turn calls for higher numerical accuracy than a similar model without a magnetic field. Hence, the assumption that electromagnetic damping of convective flows would make computations easier is wrong. At the moderate Hartmann numbers considered, stabilization of the flow takes place without significant damping of the con-

vective circulation. This leads to the need for an accurate resolution of the convective flow at a relatively high Grashof number and of the corresponding most dangerous perturbation.

IV. RESULTS

With a magnetic field absent, at aspect ratio $A=4$ and Prandtl number $Pr=0.015$, stable steady-state flows comprise two branches¹⁴ differing in the number (one or two) of main convective rolls, as illustrated in Figs. 2 and 3. Following the methodology of our previous study,¹⁴ we consider the effect of the magnetic field on each steady-state branch separately.

The Hartmann number considered does not exceed $Ha=20$. For liquid metals and semiconductors, assuming the characteristic length 0.1 m, this corresponds to the magnetic field strength 0.1–0.2 T. As calculations for $\alpha=-30^\circ$ and -60° showed that the behavior of the marginal stability curves, the patterns of the most dangerous perturbations and slightly supercritical flows are similar to those for positive values of α , we report results only for the latter. It should be noted, however, that the results for α and $-\alpha$ do not coincide for $0^\circ < \alpha < 90^\circ$.

A. Single-cell flows

The dependence of the critical Grashof number and critical oscillation frequency on the Hartmann number (i.e., the magnitude of the magnetic field) and on the orientation of the field is shown in Fig. 6. Several fixed orientations, namely $\alpha=0^\circ, 30^\circ, 45^\circ, 60^\circ$ and 90° , were considered. The marginal stability curves $Gr_{cr}(Ha)$ are nonmonotonic and consist of several continuous branches corresponding to different modes of the most dangerous perturbations described by the distinct eigenvalues of the linear stability problem.¹⁷ The dependence $\omega_{cr}(Ha)$ consists of distinct continuous curves (the imaginary parts of the distinct eigenvalues), such that each curve matches a corresponding continuous branch of $Gr_{cr}(Ha)$. Overlapping of the $\omega_{cr}(Ha)$ curves corresponds to the hysteresis loops of the $Gr_{cr}(Ha)$. The cases shown in Figs. 2, 4 and 7 are indicated by points F_2 , F_4 and F_7 , respectively, in Fig. 6(a) with the subscript for the point representing the figure number. The cases shown in Figs. 5 and 8 correspond to Grashof numbers outside the range of Fig. 6(a).

It is seen in Fig. 6(a) that at $Ha \leq 20$ there is a considerable difference in the stabilization of the flow (increase of Gr_{cr} with Ha) for magnetic fields close to horizontal ($\alpha=0^\circ$) as against fields with a significant vertical component ($\alpha \geq 30^\circ$). Under the horizontal field (with the electromagnetic force counter directional to the vertical velocity) the critical Grashof number increases monotonically with the Hartmann number from $Ha=0$ up to $Ha=12$. In the interval $12 \leq Ha \leq 17$, Gr_{cr} continue to increase steeply, exhibiting a hysteresis behavior. A further increase of Ha leads to a decrease of the critical Grashof number, due to the onset of instability in the boundary layers near the vertical boundaries. Calculations with larger Hartmann numbers ($20 \leq Ha \leq 40$) showed that the critical Grashof number behaves similarly to the $Gr(Ha)$ curves for $\alpha \geq 30^\circ$ and reaches the value

3.6×10^7 at $Ha=40$ (not shown on the graph). However, as was emphasized above, convergence of the critical parameters for $Ha > 20$ is extremely slow and the accuracy of the last result is not certain.

For $\alpha \geq 30^\circ$ when the magnetic field has a nonzero vertical component, the marginal stability curves [Fig. 6(a)], and those of the critical frequency [Fig. 6(b)] become similar in shape. For a given Hartmann number the strongest stabilization effect is associated with the vertical magnetic field ($\alpha=90^\circ$) except for the interval $6 < Ha < 7$ in which part of the hysteresis loop corresponding to $\alpha=60^\circ$ is located above its counterpart for $\alpha=90^\circ$ [Fig. 6(a)]. The similar behavior and the strongest impact of the vertical field, are apparently the consequence of interaction of the field with the horizontal velocity. As was already mentioned, the latter reaches larger values than its vertical counterpart, therefore the damping action of the vertical field component is stronger.

All marginal stability curves corresponding to $\alpha \geq 30^\circ$ show a rapid increase of the critical Grashof number with rather deep hysteresis loops in certain intervals of the Hartmann number, located according to the orientation of the magnetic field. Inside these loops the critical Grashof number is almost halved with an increase of the Hartmann number. This means that moderate field magnitudes (i.e., at $Ha \leq 10$) make for better stabilization of the flow than the higher ones (larger Ha). It should also be noted that when the field orientation changes from vertical ($\alpha=90^\circ$) to horizontal ($\alpha=0^\circ$) the hysteretic behavior of the critical Grashof number is delayed for higher Ha values. Changes in the critical parameters are smaller at values of α close to 90° and become larger below 30° .

Snapshots of the slightly supercritical oscillatory states are shown in Figs. 7 and 8. The oscillatory states were approximated asymptotically, using the weakly nonlinear exploration of the Hopf bifurcation,¹⁷ a technique successfully applied to the study of slightly supercritical convective flows.^{14,16} The oscillatory flows shown in Figs. 7 and 8 correspond to the cases considered for the convergence study, namely $Ha=20$ with $\alpha=0^\circ$ (Table II and Figs. 4) and $Ha=10$ with $\alpha=90^\circ$ (Table III and Fig. 5). In the case of the horizontal field of Fig. 7 the oscillations are most pronounced near the vertical boundaries, as it follows from the pattern of the most dangerous perturbation shown in Fig. 4. In the case of the vertical field the streamlines remain almost unchanged throughout the period of oscillations shown in Fig. 8(a). However, there are strong oscillations of the horizontal velocity in the boundary layers located near the horizontal boundaries [without significant oscillations in the core region; see Fig. 8(b)]. Oscillations of the vertical velocity are most pronounced in the central region shown in Fig. 8(c), but their largest amplitude (without strong changes in the isolines) is located near the vertical boundaries.

B. Two-cell flows

The effect of the magnetic field on the two-cell flows differs from the single-cell case. The corresponding stability diagram is shown in Fig. 9. Examples of flow and perturbation patterns are given in Figs. 10 and 11, with an example of

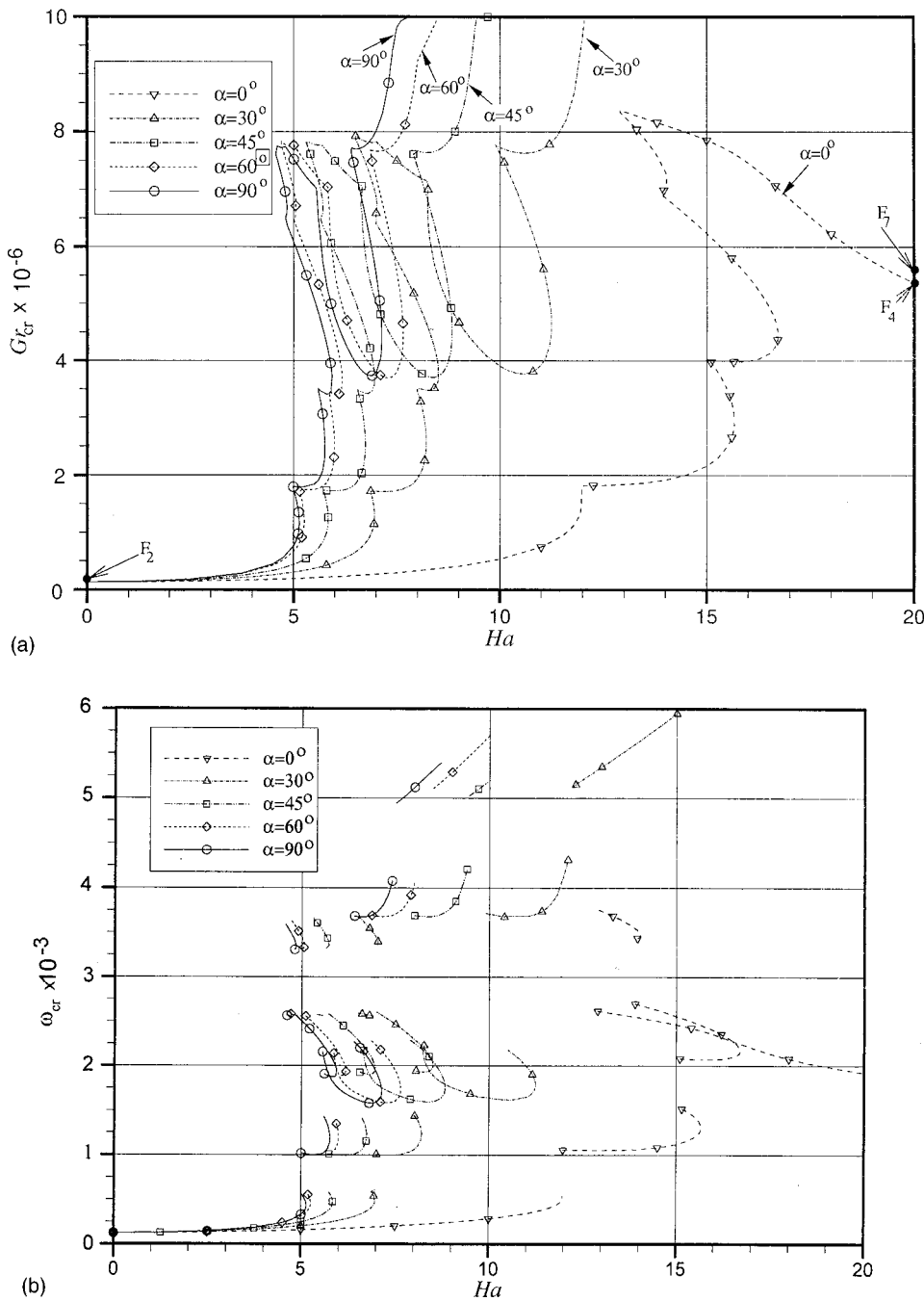


FIG. 6. Stability diagram for steady *single-cell* flows. Dependence of the critical Grashof number (a) and critical frequency (b) on the Hartmann number and field orientation. Points F_2 , F_4 and F_7 represent the cases illustrated in Figs. 2, 4 and 7, respectively.

a supercritical oscillatory state in Fig. 12. As in the preceding section, points F_3 , F_{10} , F_{11} and F_{12} correspond to the cases illustrated in Fig. 3 and Figs. 10–12.

In the two-cell flow case the maximal magnitudes of the horizontal and vertical velocities do not differ as much as in the case of single-cell flows. Accordingly, the effect of different orientation of the magnetic field is similar, as shown in Fig. 9. For each orientation the two-cell flows are stable inside the corresponding marginal stability curve shown in Fig. 9(a). The upper continuous part of the curves corresponds to the transition from steady to oscillatory two-cell flow due to a supercritical Hopf bifurcation. With an increase of the

Hartmann number, after the break on the marginal stability curves in Fig. 9(a), the Hopf bifurcation becomes subcritical. The steady-state flow and the bifurcation patterns characteristic of these two branches of the marginal stability curves are shown in Figs. 10 and 11 and correspond to points F_{10} and F_{11} in Fig. 9(a).

In case of the subcritical bifurcation, at lower values of Ha , the supercritical flow results in an asymptotically stable oscillatory two-cell pattern, while at higher values after several two-cell oscillations it transforms into a single-cell (steady or oscillatory) pattern. Such a transformation was observed when the complete unsteady problem, given by

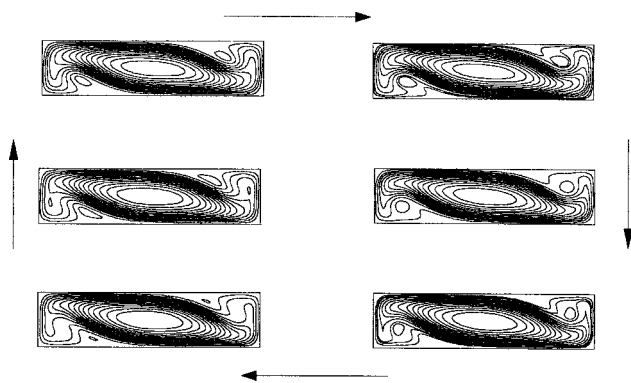


FIG. 7. Horizontal magnetic field. $Ha=20$, $\alpha=0^\circ$, $Gr=5.50 \times 10^6$ [point F_7 in Fig. 6(a)]. Instantaneous streamlines plotted for equal time intervals covering the complete period $T=3.3 \times 10^{-3}$.

Eqs. (3) through (9), was solved (by the finite volume method) for $Ha=5$, $\alpha=90^\circ$, $Gr=3.55 \times 10^6$. This is just above the critical value $Gr_{cr}=3.53 \times 10^6$ on the right-hand branch of the corresponding marginal stability curve with $\alpha=90^\circ$ as indicated by point F_{11} in Fig. 9(a). In this case the resulting single-cell flow retains its own oscillations. Note that according to the stability diagram of the single-cell flows shown in Fig. 6(a), the considered Grashof number is supercritical and the flow should indeed be oscillatory.

Figure 9(b) shows that with an increase of the Hartmann number the critical frequency rapidly tends to zero. At a certain value of Ha the marginal stability curves turn to the left and return to the axis $Ha=0$, as is seen in Fig. 9(a). These lower parts of the curves correspond to the reverse transition from two-cell to single-cell flows, which takes place due to the saddle-node bifurcation. This transition was already described in our previous study.¹⁴ Points on the neutral curves corresponding to the replacement of the Hopf bifurcation by the former are marked \times in Fig. 9(a).

The difference in the effect of the magnetic field on flows with one or two circulations is clearly seen from the patterns of the most dangerous perturbations shown in Figs. 10 and 11 (cf. the patterns shown in Figs. 4 and 5). The two-cell flows become unstable at relatively low Hartmann numbers, i.e., $Ha < 12$, such that the Hartmann boundary layers do not develop. At higher Hartmann numbers these flows are not observed. As is seen from the perturbation patterns shown in Figs. 10 and 11, the onset of instability affects the central part of the flow between the main convective cells. Similar perturbation patterns were observed for multi-cell flows without the magnetic field (compare Figs. 3 and 10). The resulting oscillations, approximated asymptotically via weakly nonlinear analysis,¹⁷ are illustrated in Fig. 12. The oscillations of two convective cells reach maximal amplitude at the center of the cavity and are similar to those observed without the magnetic field.¹⁴

Since the two-cell patterns (steady as well as oscillatory) are not observed at high Hartmann numbers it can be summed up that under the action of a sufficiently strong electromagnetic force the cellular flow transforms into a single-cell one, for which a strong stabilization effect is observed.

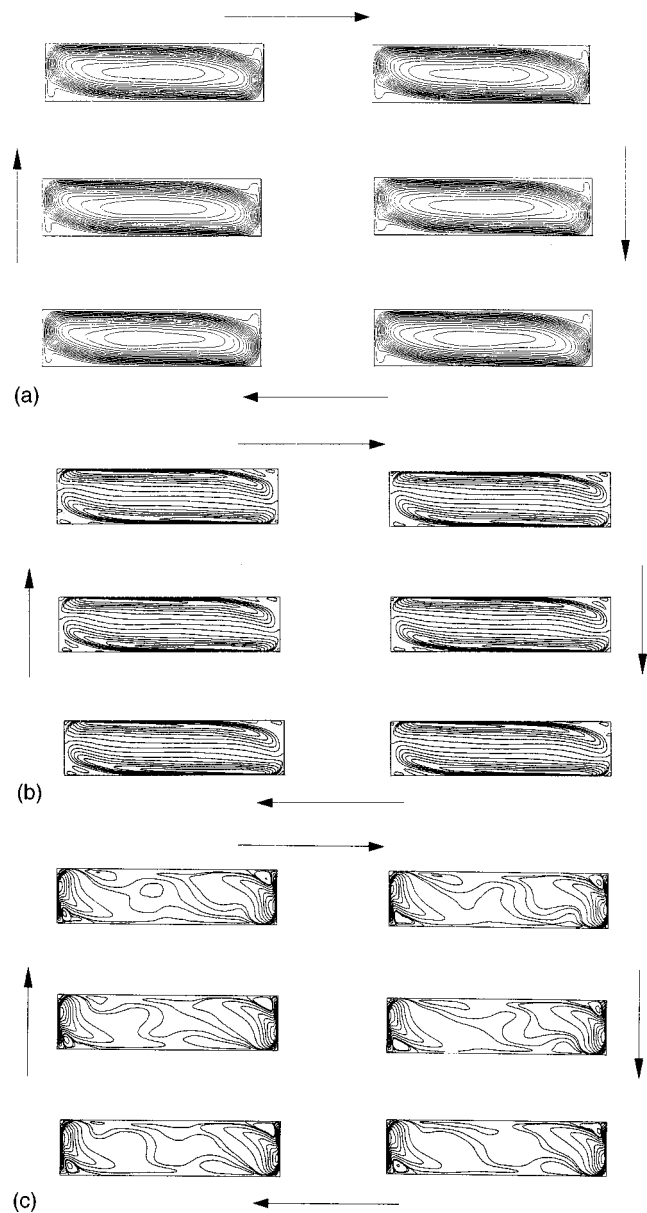


FIG. 8. Vertical magnetic field. $Ha=10$, $\alpha=90^\circ$, $Gr=1.80 \times 10^7$. Instantaneous streamlines (a), isolines of horizontal (b) and vertical (c) velocities plotted for equal time intervals covering the complete period $T=9.95 \times 10^{-3}$.

V. CONCLUSIONS

The effect of an externally imposed uniform magnetic field differs according to the flow pattern of the convective flow considered. The single-cell flow can be effectively stabilized by such a magnetic field. For horizontally elongated cavities the strongest stabilization effect is provided by a vertical field. However, at the moderate field magnitudes considered ($Ha \leq 20$) the behavior of the marginal stability curves $Gr_{cr}(Ha)$ is nonmonotonic and involves rather deep hysteresis loops where the critical Grashof number decreases with an increase of the Hartmann number. Thus, the most unexpected conclusion of the present study is the possibility of considerable destabilization of the flow by an increasing magnetic field of moderate magnitude. This leads to the problem of optimal (from the stabilization viewpoint) mag-

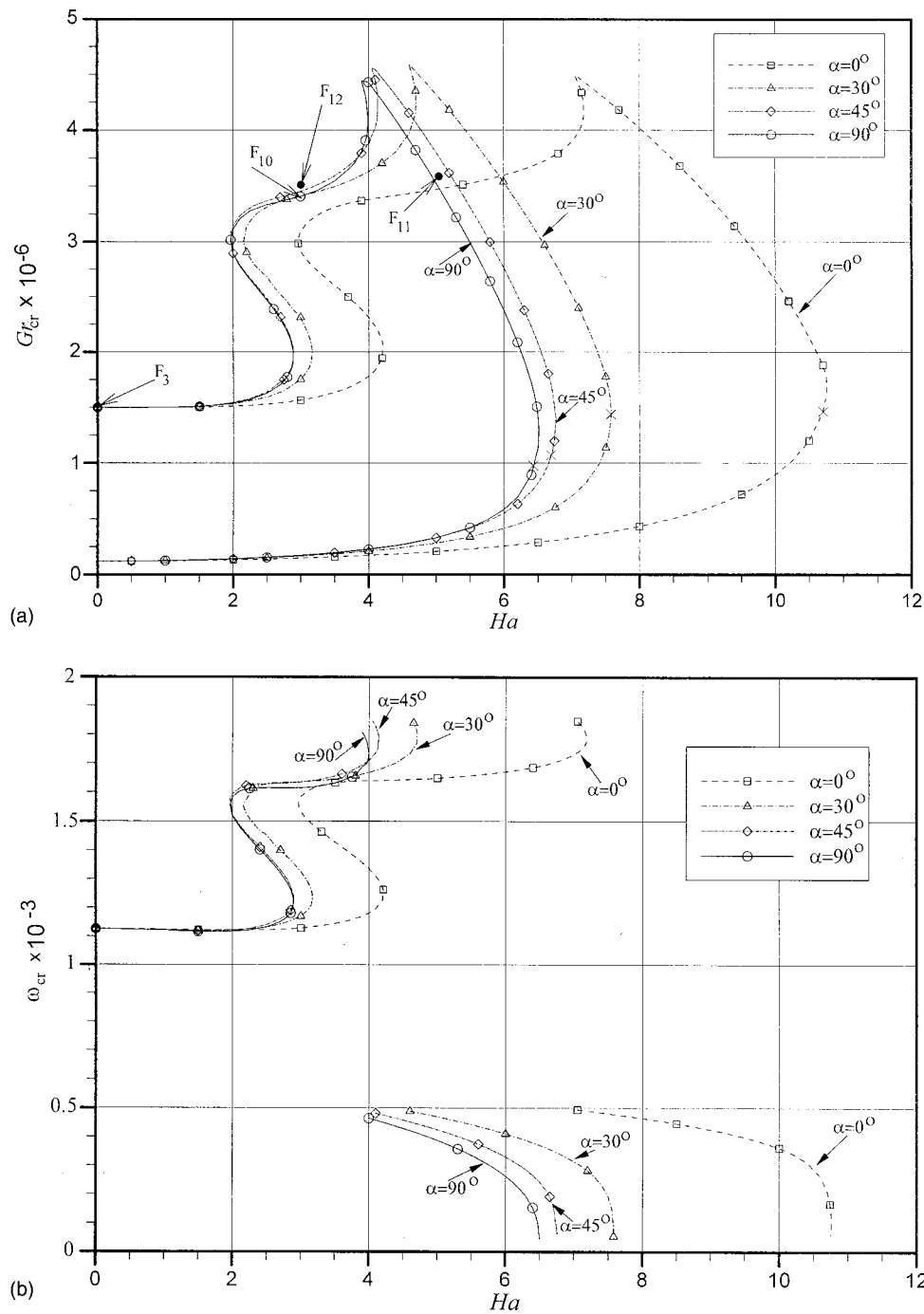


FIG. 9. Stability diagram for steady two-cell flows. Dependence of the critical Grashof number (a) and critical frequency (b) on Hartmann number and field orientation. Points F_3 , F_{10} , F_{11} and F_{12} represent the cases illustrated in Fig. 3 and Figs. 10–12, respectively.

nitude of the field, which depends on the governing parameters of the problem. It is seen also that the perturbations are suppressed before a significant reduction of the basic state flow takes place.

The effect of the magnetic field on two-cell flows is quite different. At small values of the Hartmann number the stabilization effect is not very strong. However, as the field magnitude increases these flows are destabilized and transform into single-cell ones, subject to their own stability properties. This indicates the possibility of using the magnetic field for control not only of the stability but also of the flow

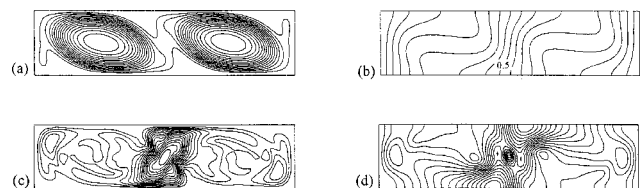


FIG. 10. Two-cell flow under the vertical magnetic field at the critical Grashof number. $Ha=3$, $\alpha=90^\circ$, $Gr_{cr}=3.41 \times 10^7$ [point F_{10} in Fig. 9(a)]. All contours are equally spaced. (a) Streamlines, $\psi_{min}=-0.933$, $\psi_{max}=294.31$; (b) isotherms, $0 \leq \theta \leq 1$; (c) amplitude of the most dangerous perturbation of the stream function; (d) amplitude of the most dangerous perturbation of the temperature.

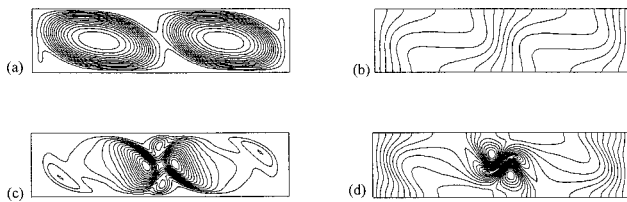


FIG. 11. Two-cell flow under the vertical magnetic field at the critical Grashof number. $Ha=5$, $\alpha=90^\circ$, $Gr_{cr}=3.53 \times 10^7$ [point F_{11} in Fig. 9(a)]. All contours are equally spaced. (a) Streamlines, $\psi_{min}=-0.655$, $\psi_{max}=291.69$; (b) isotherms, $0 \leq \theta \leq 1$; (c) amplitude of the most dangerous perturbation of the stream function; (d) amplitude of the most dangerous perturbation of the temperature.

pattern—by suppression of the multiplicity of possible steady states. We expect a similar effect for multiple steady-state flows consisting of three and more convective cells, whose stability without the magnetic field was studied previously.¹⁴

In the single-cell flows the electromagnetic damping leads to the development of the Hartmann boundary layers, as well as to boundary layers adjoining the walls parallel to the magnetic field. These layers, whose depth decreases proportionally to Ha^{-1} and $Ha^{-1/2}$, respectively, should be accounted for in any numerical model used for such flows, as it is found that the oscillatory instability sets in inside them. A significant slowdown of the numerical convergence, reflecting the need to resolve the boundary layers, can be expected at large Hartmann numbers.

It should be emphasized that the model considered was simplified as much as possible with a view to investigating the main effects of the externally imposed magnetic field on the stability of a free convective flow. Further study will involve three-dimensional models with a nonuniform (and possibly alternating) magnetic field. However, it was already shown¹⁴ that the critical parameters calculated for two-dimensional cavities compare well with the experimental results in cases where the experimental box is sufficiently long in the third direction. The conclusions derived here on the basis of a two-dimensional model should be qualitatively the

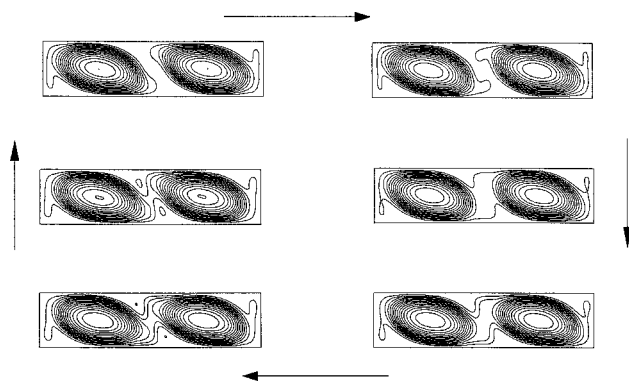


FIG. 12. Two-cell oscillatory flow in the vertical magnetic field. $Ha=3$, $\alpha=90^\circ$, $Gr=3.5 \times 10^7$ [point F_{12} in Fig. 9(a)]. Instantaneous streamlines plotted for equal time intervals covering the complete period $T=0.0043$.

same for three-dimensional ones and for those involving more complicated flow regions.

ACKNOWLEDGMENTS

This work was supported by the Israel Ministry of Science under Grant No. 8575-1-98, by the Israel Ministry of Immigrant Absorption (to A.G.), by the Y. Winograd Chair of Fluid Dynamics and Heat Transfer, and by the Israel High Performance Computer Unit.

- ¹D. T. J. Hurle, "Temperature oscillations in molten metals and their relationship to growth striae in melt-grown crystals," *Philos. Mag.* **101**, 305 (1966).
- ²D. T. J. Hurle, E. Jakeman, and C. P. Johnson, "Convective temperature oscillations in molten gallium," *J. Fluid Mech.* **64**, 565 (1974).
- ³D. T. J. Hurle and R. W. Series, "Use of a magnetic field in melt growth," in *Handbook of Crystal Growth*, edited by D. T. J. Hurle (North-Holland, Amsterdam, 1994), Vol. 2, p. 711.
- ⁴M. Seki, H. Kawamura, and K. Sanokawa, "Natural convection of mercury in a magnetic field parallel to the gravity," *J. Heat Transfer* **101**, 227 (1979).
- ⁵K. Okada and H. Ozoe, "Experimental heat transfer rates of natural convection of molten gallium suppressed under an external magnetic field in either the X, Y, or Z direction," *J. Heat Transfer* **114**, 107 (1992).
- ⁶A. Juel, T. Mullin, H. Ben Hadid, and D. Henry, "Magnetohydrodynamic convection in molten gallium," *J. Fluid Mech.* **378**, 97 (1999).
- ⁷T. Tagawa and H. Ozoe, "Enhancement of heat transfer rate by application of a static magnetic field during natural convection of liquid metal in a cube," *J. Heat Transfer* **119**, 265 (1997).
- ⁸H. Ben Hadid, D. Henry, and S. Kaddeche, "Numerical study of convection in the horizontal Bridgman configuration under the action of a constant magnetic field. Part 1. Two-dimensional flow," *J. Fluid Mech.* **333**, 23 (1997).
- ⁹H. Ben Hadid and D. Henry, "Numerical study of convection in the horizontal Bridgman configuration under the action of a constant magnetic field. Part 2. Three-dimensional flow," *J. Fluid Mech.* **333**, 57 (1997).
- ¹⁰R. Mößner and U. Müller, "A numerical investigation of three-dimensional magnetoconvection in rectangular cavities," *Int. J. Heat Mass Transf.* **42**, 1111 (1999).
- ¹¹R. Bessaih, M. Kadja, and Ph. Marty, "Effect of wall electrical conductivity and magnetic field orientation on liquid metal flow in a geometry similar to the horizontal Bridgman configuration for crystal growth," *Int. J. Heat Mass Transf.* **42**, 4345 (1999).
- ¹²K. E. McKell, D. S. Broomhead, and D. T. J. Hurle, "Torus doubling in convecting molten gallium," *Europhys. Lett.* **12**, 513 (1990).
- ¹³L. Davoust, R. Moreau, and R. Bolcato, "Control by a magnetic field of the instability of Hadley circulation in a low-Prandtl-number fluid," *Eur. J. Mech. B/Fluids* **18**, 621 (1999).
- ¹⁴A. Yu. Gelfgat, P. Z. Bar-Yoseph, and A. L. Yarin, "Stability of multiple steady states of convection in laterally heated cavities," *J. Fluid Mech.* **388**, 315 (1999).
- ¹⁵A. Yu. Gelfgat and I. Tanasawa, "Numerical analysis of oscillatory instability of buoyancy convection with the Galerkin spectral method," *Numer. Heat Transfer, Part A* **25**, 627 (1994).
- ¹⁶A. Yu. Gelfgat, P. Z. Bar-Yoseph, and A. L. Yarin, "On oscillatory instability of convective flows at low Prandtl number," *J. Fluids Eng.* **119**, 823 (1997).
- ¹⁷A. Yu. Gelfgat, "Two- and three-dimensional instabilities of confined flows: numerical study by a global Galerkin method," *Comput. Fluid Dyn. J.* **9**, 437 (2000).
- ¹⁸B. Roux (ed.), "Numerical simulation of oscillatory convection in low-Pr fluids: A GAMM workshop," *Notes on Numerical Fluid Mechanics* (Vieweg, Braunschweig, 1990), Vol. 27.
- ¹⁹A. Yu. Gelfgat, "Effects of the magnetic field magnitude and direction on the oscillatory thermogravitational convection regimes in a rectangular cavity," *Magnetohydrodynamics (N.Y.)* **24**, 324 (1988).
- ²⁰P. H. Roberts, *An Introduction to Magnetohydrodynamics* (Longmans, London, 1967).
- ²¹L. Davoust, M. D. Cowley, R. Moreau, and R. Bolcato, "Buoyancy-driven convection with a uniform magnetic field. Part 2. Experimental investigation," *J. Fluid Mech.* **400**, 59 (1999).